Peierls Potential for Crowdions in the bcc Transition Metals

S. P. Fitzgerald and D. Nguyen-Manh
EURATOM/UKAEA Fusion Association, Culham Science Centre, Abingdon, OX14 3DB, United Kingdom
(Received 18 April 2008; published 11 September 2008)

We present the first derivation of the analytic expression for the Peierls-Nabarro potential for crowdion migration using the double sine-Gordon model. The analysis is guided by the group-specific trend in the shapes of the periodic lattice potentials calculated for the body-centered-cubic transition metals in groups 5B and 6B of the periodic table. We combine density-functional calculations of the crowdion's profile and environment with an extended version of the analytical Frenkel-Kontorova model, and determine the effective potential experienced by the defect's center of mass. This reveals important underlying differences between the metals in these groups, which are inaccessible to either the numerical or analytical approaches alone, and accounts for the previously unexplained significantly higher crowdion migration temperatures observed in the metals of group 6B relative to those of group 5B.

DOI: 10.1103/PhysRevLett.101.115504 PACS numbers: 61.72.Bb, 61.72.jj, 71.55.Ak

Self-interstitial atom (SIA) defects are produced in crystalline materials under irradiation. Body-centered-cubic (bcc) transition metals and their alloys (especially tungsten and ferritic-martensitic steels) are the leading candidate materials for fusion and advanced fission power plants, and a quantitative understanding of SIA formation and migration behavior is essential if we wish to accurately model the microstructural evolution of these materials [1]. Experimental data for the onset of long-range migration of SIAs, obtained mostly from resistivity recovery measurements following electron irradiation, show a remarkable group-specific trend depending upon the electron-to-atom ratio. For group 5B of the bcc transition metals (V, Nb, and Ta), the resistivity data indicate that SIAs are already mobile at the irradiation temperature, usually about 6 K, whereas for the elements of group 6B, the temperature for the onset of long-range migration is 40 K for Cr, 35 K for Mo, and 27 K for W [2]. Recent systematic density-functional theory (DFT) studies of the formation energies of point defects, spanning the entire group of bcc metals, reveal that the single SIA defects of all nonmagnetic bcc transition metals adopt a linear $\langle 111 \rangle$ crowdion configuration [3,4]. Crowdion defects consist of an additional atom inserted into a string of atoms oriented along a close-packed direction in the lattice, usually the $\langle 111 \rangle$ direction in the bcc case, and although in magnetic bcc-Fe it is not the most stable SIA defect [5–7], clusters of SIAs in Fe do adopt this configuration [1]. They are highly mobile in general because the translation along the string of the center of mass of the defect (where the associated strain is the highest) involves only very small displacements of each constituent atom. It is possible to formulate a simple analytically soluble model describing not only individual $\langle 111 \rangle$ crowdion defects [8], but also clusters thereof [9], via the Lagrangian

$$\mathcal{L} = \sum_{n=-\infty}^{\infty} \left\{ \frac{m\dot{z}_n^2}{2} - \frac{\beta}{2}(z_{n+1} - z_n - a)^2 - V(z_n) \right\}. \quad (1)$$

The sum runs over the close-packed string of atoms (mass m, positions z_n), connected by harmonic springs (constant β), interacting with the surrounding "perfect" lattice via the potential $V(z_n)$. If the displacement of each atom $u_n \equiv z_n - na$ is assumed to vary slowly along the string, it can be described by a continuous function $u(z)$, which satisfies $u(-\infty) = a$, $u(\infty) = 0$, reflecting the single additional atom in the string. (a is the equilibrium spacing of the atoms in the close-packed string, and equals $r_0\sqrt{3}/2$ for the $\langle 111 \rangle$ direction in a bcc crystal with lattice spacing r_0). Equation (1) is the Frenkel-Kontorova (FK) model, conventionally used to model one-dimensional (1D) dislocations (among other applications; for a review see [10] and references therein).

The lattice potential $V(z)$ is obviously periodic, and is conventionally taken to be proportional to $\sin^2(\pi z/a)$, which leads to a kinklike arctangent solution for the displacement field. However, as our DFT calculations demonstrate, the potential acting on the $\langle 111 \rangle$ string is not well described by a simple sine-squared function, particularly for the transition metals of group 6B. Here we consider a double-sine lattice potential of the form

$$V(z) = V_0 \left[\sin^2\left(\frac{\pi z}{a}\right) + \frac{\alpha^2 - 1}{4} \sin^2\left(\frac{2\pi z}{a}\right) \right], \quad (2)$$

which returns to the single-sine form in the limit $\alpha \to 1$. As α increases above 1 the peak flattens, and when $\alpha > \sqrt{2}$, $V(z)$ contains a local minimum at $z = a/2$ (see Fig. 1). Including this term amounts to truncating the Fourier series for the true periodic potential at second rather than first order. In the continuum limit, the Lagrangian (1) with the potential (2) has the kinklike static displacement field solution

$$u(z) = \frac{a}{\pi} \arctan\left[\frac{\alpha}{\sinh(\mu\alpha(z - z_0))} \right], \quad (3)$$

where $\mu^2 = 2\pi^2 V_0/\beta a^4$ encodes the relative strength of

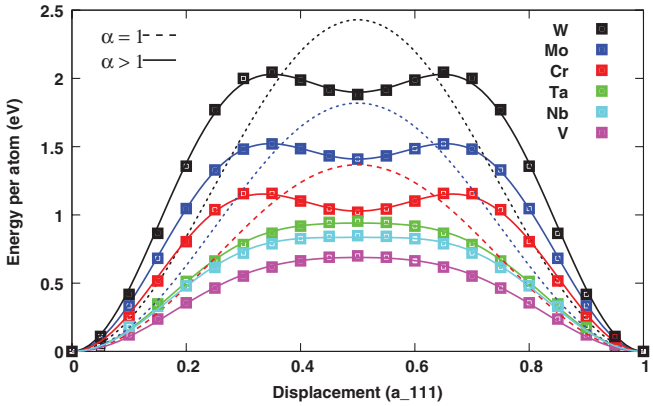

FIG. 1 (color). Energy of displaced ⟨111⟩ string in V, Nb, Ta, Cr, Mo, W. Data points: DFT total energy per atom (VASP); solid lines: fit of function V [Eq. (2)]; dashed lines: best fit of V when $\alpha = 1$ for W, Mo, Cr.

the interaction within the string (β), and the interaction with the surrounding lattice (V_0). z_0 is an arbitrary constant representing the center of mass of the crowdion. This solution was derived in [11] in the context of kinked dislocation lines. When the single-sine lattice potential is used ($\alpha \to 1$), the displacement solution becomes $u_0(z) = (2a/\pi)\arctan(\exp[-\mu(z - z_0)])$. In this case, μ has a clear physical interpretation as the inverse length scale of the defect: a smaller value of μ corresponds to a more slowly varying displacement field and a more "spread out" defect, involving more atoms than the large-μ case. When the more general potential is used, it is the combination $\alpha\mu$ which sets this scale, so a large α, corresponding to deep local minima in the lattice potential, has a similar effect to increasing V_0 in the traditional form of the potential. In the bcc transition metals considered below, this inverse length scale is always less than 1 (in inverse lattice units), though for Cr this is marginal. The crowdion's total elastic energy can be written

$$E_0 = \int_{-\infty}^{\infty} \left\{ \frac{\beta a^2}{2} \left(\frac{du}{dz} \right)^2 + V(u(z)) \right\} dz. \tag{4}$$

Substituting (3) into the above expression for the energy shows that the solution partitions the energy equally between the elastic interaction of the atoms in the string and the interaction with the surrounding lattice; i.e., the two terms in the integrand of (4) are equal [the first integral of the Euler-Lagrange equation reads $(u')^2 \sim V(u)$]. Also, since $u = u(z - z_0)$, E_0 is independent of z_0, reflecting the continuum limit being taken. Physically, this corresponds to the period of the lattice potential going to zero, and in this approximation the crowdion moves freely through the lattice (it is essentially a Goldstone mode [8,12]). The only information about $V(z)$ is that retained in the shape of the kink solution. However, lattice discreteness can play an important role, and the expression for E_0 in (4) should be viewed as a zeroth order approximation to the full discrete expression for the energy [8]

$$E = \sum_{n=-\infty}^{\infty} \left\{ \frac{\beta}{2}(u_{n+1} - u_n)^2 + V(u_n) \right\} \to 2 \sum_{n=-\infty}^{\infty} V(u_n), \tag{5}$$

where the replacement follows from the equipartition property mentioned above. $u_n = u(na)$; i.e., the continuum displacement field solution is evaluated at each atom. Substituting (3) in (2) and applying the Poisson summation formula, Eq. (5) can be written as

$$E(z_0) = E_0 + \sum_{j=1}^{\infty} I_j \cos\left(\frac{2\pi j z_0}{a} \right), \tag{6}$$

a Fourier series for the position-dependent energy of the crowdion. The first term E_0 is the same as Eq. (4), and is independent of the position of the crowdion. The sum gives the potential landscape that the crowdion *as a whole* experiences, depending on the collective coordinate z_0. Arising entirely from the lattice discreteness, this is precisely analogous to the Peierls-Nabarro potential [13] experienced by an edge dislocation, and is entirely distinct from the lattice potential $V(z)$, which describes the interaction between the *individual atoms* in the string with those of the surrounding lattice.

The terms $I_j \cos(2\pi j z_0/a)$ are given by

$$4V_0\alpha^4 \int_{-\infty}^{\infty} \cos(2\pi jk) \frac{\cosh^2(\alpha\mu(ka - z_0))}{[\alpha^2 + \sinh^2(\alpha\mu(ka - z_0))]^2} dk, \tag{7}$$

which leads eventually to

$$I_j = \frac{2V_0\alpha\pi}{\mu a} \operatorname{cosech}\left(\frac{\xi\pi}{2} \right) \times \left\{ \xi \cos\left(\frac{\xi}{4} \ln\frac{q_+}{q_-} \right) - \frac{1}{\alpha\sqrt{\alpha^2 - 1}} \sin\left(\frac{\xi}{4} \ln\frac{q_+}{q_-} \right) \right\}, \tag{8}$$

where $\xi = 2\pi j/\alpha\mu a$ and $q_{+,-} = 1 - 2\alpha^2 \pm 2\alpha\sqrt{\alpha^2 - 1}$. Note the considerable simplification when the conventional lattice potential is used: on taking the limit $\alpha \to 1$, the term in braces becomes $2\xi \to 4\pi j/\mu a$ and $I_j \to 4j\beta a^2 \operatorname{cosech}(\pi^2 j/a\mu) \approx 8j\beta a^2 \exp(-\pi^2 j/a\mu)$, in agreement with Ref. [8]. In either case, since $\mu a\alpha < 1$, the cosech term suppresses the potential, explaining the small energy barriers to crowdion migration.

In order to estimate the values of the model parameters, we turn to *ab initio* calculations of the lattice potentials along the ⟨111⟩ direction shown in Fig. 1 for the bcc metals of groups 5B and 6B. These were determined by considering a defect-free lattice, and calculating the energy per atom of one of the ⟨111⟩ strings as it was rigidly displaced relative to its neighbors along its axis using DFT. This provides an accurate calculation of the periodic potential

$V(z)$ that is consistent with the 1D FK model. The DFT computations were performed self-consistently with respect to the electron charge density at fixed ionic positions; hence, the changes in the metallic bonding between the atoms as they are displaced are properly taken into account. DFT calculations performed with full ionic relaxations do not show significant deviations in the magnitude or shape of the potentials.

The Perdew-Burke-Ernzerhof [14] generalized gradient approximation for exchange and correlation functionals was used, and to ensure the DFT results are code-independent, we used two *ab initio* packages: (i) PLATO, a package of linear combinations of atomic-type orbitals [15] using the relativistic semicore separable pseudopotentials developed by Hartwigsen *et al.* [16], and (ii) VASP, a plane-wave based code using projected augmented wave potentials [17]. A description of the PLATO method for bcc transition metals is outlined in [3,4]. Standard projected augmented wave potentials provided within the VASP code were used with semicore electrons and the plane-wave energy cutoff was set to 400 eV, which is sufficient for total energy convergence in the bcc metals. A unit cell with the supercell vectors, $\vec{a}_1 = 3r_0[11\bar{2}]$, $\vec{a}_2 = 3r_0[\bar{1}10]$, and $\vec{a}_3 = (r_0/2)[111]$, was used to calculate the periodic potential along the [111] direction. The bcc lattice constants r_0 for all transition metals were predicted in our earlier DFT calculations [3,4]. Brillouin zone sampling was done using the Monkhorst-Pack scheme and the calculations were carried out with $4 \times 6 \times 12$ shifted $\boldsymbol{k}$-point grids. The quantitative results for the lattice potentials from both codes were in agreement with each other. We note that for bcc-Cr, due to the very small energy difference between the nonmagnetic and antiferromagnetic states [3,4,18], non-spin-polarized DFT calculations are shown in this study.

Figure 1 demonstrates the clear group-specific trend in the potentials, both in shape and predicted energy at the central point. For group 5B, the DFT calculations show the same structure of a flattening peak, whereas a structure with a local minimum is characteristic of the metals in group 6B. The lattice potential energy at the central displacement increases from 0.70 to 0.85 to 0.95 eV for V, Nb, and Ta, respectively, and from 1.02 to 1.41 to 1.88 eV for Cr, Mo, and W. Also shown is the function $V(z)$ of Eq. (2), fitted to the density-functional results for the six metals under consideration. This function can accurately accommodate all the features of the potentials, in particular the local minima exhibited by Cr, Mo, and W of group 6B, with a large amplitude of the second harmonic ($\alpha > \sqrt{2}$). The single-sine [8,9] form for the potential is shown (dotted line) for these three metals also, and cannot capture the additional structure. V, Nb, and Ta of group 5B are closer to the sinusoidal shape, though they still have a flattened peak which requires the form of Eq. (2) to fully describe it ($1 < \alpha < \sqrt{2}$). The difference arises from the group-specific nature of the metallic bonding and cohesive energy, which the DFT calculations reveal [3].

TABLE I. Fitted parameters and derived quantities for the metals of groups V and VI. Also given are the estimated migration temperatures T_m in kelvin, and their experimental values taken from Ref. [2].

Metal	V_0 (eV)	β (eV/a^2)	α	μ	T_m est.	T_m [2]
V	0.689	41.1	1.31	0.575	~8	<6
Nb	0.835	69.1	1.41	0.488	~0.3	<6
Ta	0.940	81.6	1.36	0.477	~0.1	<6
Cr	1.03	63.1	1.73	0.568	~100	~40
Mo	1.41	130	1.66	0.463	~30	35
W	1.90	177	1.64	0.460	~30	27

Fitting the gradient of Eq. (3) to the DFT-determined displacement gradients for ⟨111⟩ crowdions in the six metals [3,4] under consideration fixes the spring constant β, so the model is completely determined in terms of three parameters V_0, β, and α for each metal. The values are given in Table I, together with the parameter μ. The data in the last two columns are discussed below. I_1, the first Fourier coefficient in the Peierls-Nabarro potential of Eq. (8), is plotted versus α and μ in Fig. 2 (the next-to-leading coefficient is negligible across the parameter range of interest). For the single-sine lattice potential ($\alpha = 1$) the barrier is $\lesssim 10^{-5}$ eV across the range of μ. However, higher values of α allow a more pronounced variation with μ, and, in particular, a marked increase is seen when both α and μ are large. The barrier heights for V, Nb, Ta are 6.8×10^{-4}, 0.25×10^{-4}, and 0.087×10^{-4} eV, respectively, and those for Cr, Mo, W are 12×10^{-3}, 2.4×10^{-3}, and 2.6×10^{-3} eV, respectively. These values are too small to be directly computed within DFT (they are of the order of the DFT error). However, the lattice potential values are several orders of magnitude larger, and the analytical approach leading to Eq. (8) bridges the gap in scales, allowing us to indirectly calculate

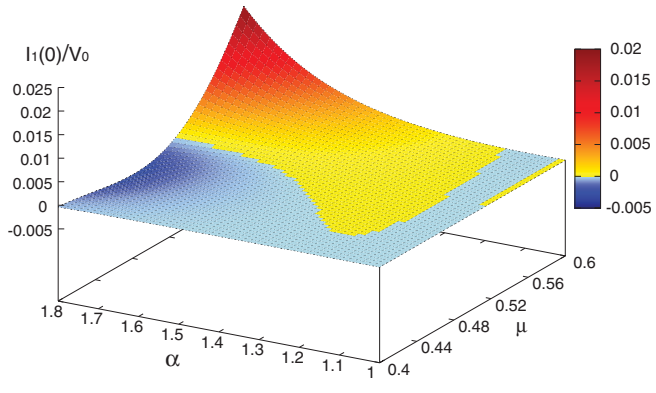

FIG. 2 (color). First Fourier coefficient of effective potential versus α and μ. (The prefactor of V_0 is divided out as we focus on the α and μ dependence.)

the small migration barriers using reliable DFT computations of much larger quantities.

The atomic positions no longer appear in the expression for the crowdion's energy (6) but, unlike in (4), their effect remains. A large value of α corresponds to deep local minima in the lattice potential. This mimics a larger value of μ in the conventional FK model: during a translation of a more localized defect's center of mass, the motion is closer in nature to the translation of the individual atoms, which leads to an increased barrier. The local minima in the double-sine lattice potential lead to more regions of alternating potential gradient; hence, more atoms experience a force resisting their motion, which has the same effect. The contour $I_1 = 0$, visible in Fig. 2, represents a relation between α and μ which gives zero barrier at leading order. The metals of group 5B lie closer to this curve than those of group 6B, so in 6B we expect a relatively higher migration temperature, as reported in [2]. These data are reproduced in Table I, along with the calculated energy barriers divided by Boltzmann's constant. This provides a very approximate estimate of the migration temperatures according to the model (only the first significant figure is given), and although they differ quantitatively, the group-specific behavior is correctly predicted. We note again that for bcc-Cr the SIA migration mechanism is likely to be more complicated since the difference between the formation energies for the crowdion and the $\langle 110 \rangle$ configuration is negligible.

In conclusion, we have used DFT to calculate the potential experienced by a $\langle 111 \rangle$ string of atoms due to neighboring strings, in the bcc transition metals of groups 5B and 6B of the periodic table. This has revealed a significant difference between the metals of the two groups, namely, the existence of a pronounced local minimum in the lattice potentials of the group 6B metals. These cannot be accurately fitted by a single-sine function; however, the inclusion of the second harmonic in the function can fully describe the potential for all six metals under consideration. A FK model for $\langle 111 \rangle$ crowdions can be applied with this generalized potential, and the three parameters of the model were determined via fits to the DFT calculations of the potentials and displacement fields. When the effects of lattice discreteness are taken into account, the Peierls potential experienced by the defect's center of mass can be determined (this is zero when discreteness is neglected, and generally too small to be directly estimated using DFT). This analytical calculation reveals the impact a local minimum in the lattice potential can have on the defect's migration: a deep local minimum leads to a significantly enhanced barrier to migration. This can explain the observed large differences in the crowdion migration temperatures between groups 5B and 6B, as measured in resistivity recovery experiments [2]. A more quantitative estimate of these temperatures could be made by calculating the escape rates, which would require taking several other factors into account, particularly the defect's effective mass and lattice friction. However, the results presented here explain the key difference between the groups and provide estimates of the migration barrier for each metal in broad agreement with experimental measurements. Since an edge dislocation can be thought of as a suitable ensemble of crowdions [9], this work suggests that edge dislocation mobility should follow a similar group-specific pattern.

The authors thank S. Dudarev and A. Thyagaraja for stimulating discussions. This work is supported by the U.K. Engineering and Physical Sciences Research Council, by EURATOM, and by EXTREMAT integrated project under Contract No. NMP3-CT-2004-500253.

[1] K. Arakawa, K. Ono, M. Isshiki, K. Mimura, M. Uchikoshi, and H. Mori, Science **318**, 956 (2007).
[2] P. Ehrhart, P. Jung, H. Shultz, and H. Ullmaier, in *Atomic Defects in Metals*, edited by H. Ullmaier Landolt-Bornstein New Series, Group III, Vol. 25 (Springer-Verlag, Berlin, 1991).
[3] D. Nguyen-Manh, A. P. Horsfield, and S. L. Dudarev, Phys. Rev. B **73**, 020101(R) (2006).
[4] P. M. Derlet, D. Nguyen-Manh, and S. L. Dudarev, Phys. Rev. B **76**, 054107 (2007).
[5] C. C. Fu, F. Willaime, and P. Ordejon, Phys. Rev. Lett. **92**, 175503 (2004).
[6] G. Liu, D. Nguyen-Manh, B. G. Liu, and D. G. Pettifor, Phys. Rev. B **71**, 174115 (2005).
[7] D. Nguyen-Manh, V. Vitek, and A. P. Horsfield, Prog. Mater. Sci. **52**, 255 (2007).
[8] A. M. Kosevich, *The Crystal Lattice* (Wiley-VCH, New York, 1999).
[9] S. L. Dudarev, Philos. Mag. **83**, 3577 (2003).
[10] O. M. Braun and Y. S. Kivshar, *The Frenkel-Kontorova Model* (Springer, New York, 2004).
[11] F. C. Frank and J. H. van der Merwe, Proc. R. Soc. A **200**, 125 (1949).
[12] S. L. Dudarev, Phys. Rev. B **65**, 224105 (2002).
[13] R. Peierls, Proc. Phys. Soc. London **52**, 34 (1940).
[14] J. P. Perdew, K. Burke, and M. Ernzerhof, Phys. Rev. Lett. **77**, 3865 (1996).
[15] S. D. Kenny, A. P. Horsfield, and H. Fujitani, Phys. Rev. B **62**, 4899 (2000).
[16] C. Hartwigsen, S. Goedecker, and J. Hutter, Phys. Rev. B **58**, 3641 (1998).
[17] G. Kresse and J. Hafner, Phys. Rev. B **47**, 558 (1993); G. Kresse and J. Furthmuller, *ibid.* **54**, 11 169 (1996); G. Kresse and D. Joubert, *ibid.* **59**, 1758 (1999).
[18] S. Frederiksen and K. W. Jacobsen, Philos. Mag. **83**, 365 (2003).